Proper Orthogonal Decomposition (POD) of the Wake Flow Field of a Model Wind Turbine and a Porous Disc under Different Freestream Turbulence Intensity Conditions

Proper Orthogonal Decomposition (POD) of the Wake Flow Field of a Model Wind Turbine and a Porous Disc under Different Freestream Turbulence Intensity Conditions

Buğrahan ÖZTÜRK[1,2], Abdelrahman HASSANEIN[1], M Tuğrul Akpolat[1], Anas ABDULRAHIM[3], Mustafa PERÇİN[1,2] and Oğuz UZOL[1,2]

[1] Department of Aerospace Engineering, Middle East Technical University (METU), Ankara, Turkey
[2] METU Center for Wind Energy Research (RÜZGEM), METU, Ankara, Turkey
[3] Turkish Aerospace Industries, Experimental Aerodynamics, Ankara, Turkey

uzol@metu.edu.tr

Abstract. The effects of freestream turbulence intensity on the wake development of a model wind turbine and a porous disc are investigated through Proper Orthogonal Decomposition (POD) analysis. The capability of porous discs for reproducing far-wake characteristics of a model wind turbine is examined through coherent structures both in the near-wake and far-wake regions. Instantaneous velocity fields are obtained through wake measurements using two-dimensional two-component particle image velocimetry (2D2C PIV). These velocity fields are considered snapshots of the spatial domain. Results show inherent differences between coherent structures of a model wind turbine and porous disc in the near-wake region, especially when the freestream turbulent intensity level is low. However, these differences reduce, and coherent structures become more comparable when the freestream turbulence intensity level is higher. It is shown that the first five streamwise components of POD modes are paired for the model wind turbine and the porous disc cases under high freestream turbulence intensity conditions in the far-wake region.

1. Introduction

Power losses occur in wind farms due to wind turbines operating in the wake of upstream turbines. These wakes are characterized by increased velocity deficits and higher turbulence intensities which result in lower energy extraction from the wind and increased fatigue loading on downstream turbines [1]. Therefore, a comprehensive understanding of the phenomena associated with wind turbine wakes

is essential to optimize performance and reduce power losses. In this respect, numerous studies have been performed, ranging from field measurements [2], numerical simulations [3], and wind tunnel studies [4].

In wind tunnel studies, porous discs are frequently used to represent the wakes of wind turbines, mainly for the far wake region. In the near wake, the porous disc fails to reproduce the wake characteristics. This is due to the helical instability of the tip vortices, which affects the mixing process of the entire wake [5]. Several studies have been performed to compare the wakes between model wind turbines and porous discs. For instance, Aubrun et al. [6] performed a wind tunnel study to compare the wake development characteristics of a model wind turbine and a porous disc under two inflow conditions, namely decaying isotropic inflow and atmospheric boundary layer. Results show that the porous disc is able to reproduce similar far-wake characteristics with the model wind turbine beyond three diameters downstream under atmospheric boundary layer conditions when ambient turbulence intensity is adequately high. Camp and Cal [7] performed a wind tunnel study to investigate the similarities in terms of mean kinetic energy transport inside the wind farm by examining the wake of the center model in the last row of a 4x3 array. Results show that, although notable differences occur in the near-wake due to the absence of the blades, porous discs can be employed to recreate the far-wake characteristics of wind turbines. Furthermore, Lignarolo et al. [8] conducted an experimental study comparing a model wind turbine and a porous disc under uniform inflow with low turbulence intensity to exclude wake-induced mixing features in the near-wake region. Results reveal that both models have similar wake expansion and energy reduction in the near-wake region but have different turbulent mixing characteristics.

Proper Orthogonal Decomposition (POD) is a statistical tool that is used to investigate coherent structures in turbulent flows and quantitatively distribute these structures based on their energy content. In other words, organized motions that constitute little energy are not important statistically but may have dynamic significance and are restricted to high-rank modes [9]. Consequently, the flow field can be reconstructed using the least number of higher energy modes. Lumley [10,11] initially introduced the POD technique to turbulent flow problems to study coherent structures in turbulence. Sirovich [12] later on developed the Snapshot POD, which is better suited for spatially dense but temporally sparse data.

In recent years the POD found many applications for studying turbulent wakes downstream of wind turbines and within wind farms based on the results of several numerical and experimental studies. For instance, Andersen et al. [13] simulated a wind farm using infinitely long rows of turbines by employing large eddy simulation coupled with the actuator line technique. POD was implemented to analyze the key turbulent features in the wake downstream of wind turbines under idealized inflow conditions (i.e., no freestream turbulence or shear). Results show that POD can give insight into the relationship between the dynamic wake meandering and wind turbine spacing as well as vortex shedding from upstream turbines. VerHulst and Meneveau [14] also employed POD to reveal the most energetic flow structures in a wind farm. Counter-rotating vortex pairs above the height of the wind turbines were observed, which amount to around 14% of the mean kinetic energy within the wake. De Cillis et al. [15] employed POD analysis to a numerical wake dataset obtained through LES coupled with the actuator line method to investigate the wake recovery of a single wind turbine. Results show that the presence of tip vortices delays wake recovery, while flow structures induced from the tower has a good influence on wake recovery. Bastine et al. [16] argued that only a few modes are necessary to capture the basic dynamical aspects of the wake of a single wind turbine immersed inside an ABL inflow. Camp and Cal [9] carried out similar wind tunnel studies on an array of wind turbines and an equivalent array of porous discs. POD results reveal differences in the organization of the turbulent kinetic energy of the wake structure of the wind turbines and porous discs. For instance, they observed that the first mode of the streamwise and vertical components is similar spatially for the rotor and disc in both the near and far wake, unlike the cross-stream component.

Recently, Öztürk et al. [17] performed measurements to show freestream turbulence intensity effects on wake development downstream of a model wind turbine and a porous disc with similar thrust coefficients. Results show that difference in the wake velocity deficit in the far-wake decreases between

the two rotor models as the freestream turbulence intensity level increases. The present study is an extension of Öztürk et al. [17], and it provides POD analysis of the wake flow field of a model wind turbine and a porous disc with similar thrust coefficients under different freestream turbulence intensity levels. The main focus of this study is to demonstrate the effects of freestream turbulence on wake coherent structures of the two rotor models. Measurements are conducted using two-dimensional two-component particle image velocimetry (2D2C PIV) within the wakes of a model wind turbine and a porous disc of similar diameter and thrust coefficient under different freestream turbulence intensity levels.

2. Methodology

2.1. Wind Tunnel Facility and Experimental Models

The wake measurements are performed inside an open-return wind tunnel located at the METU Center for Wind Energy Research (RÜZGEM). This wind tunnel utilized for experiments has an 8 m long test section composed of plexiglass walls with 1×1 m^2 cross-sectional area. At the test section inlet, the maximum velocity and turbulence intensity levels are around 25 m/s and less than 0.35%, respectively. For the constant Reynolds number operation, an in-house closed-loop wind tunnel control system is used. Figure 1a shows the wind tunnel used in the experiments. The three-bladed horizontal axis model wind turbine and the porous disc used in the present study are comparable to those used in Camp and Cal [7]. The cross-section of the model wind turbine is linearly tapered, with a twist angle of 22º at the root and 15º at the tip. The porous disc with the same diameter and similar thrust coefficient as the model wind turbine has non-uniform porosity in the radial direction. An ATI Gamma Force/Torque sensor installed beneath the tower outside the wind tunnel was used to measure the thrust of the porous disc and the model wind turbine under different levels of freestream turbulence intensity. The wind turbine rotational speed is adjusted in accordance with the thrust coefficient of the porous disc after first determining the thrust coefficient of the porous disc. The model wind turbine in this study is run at a constant speed of 4250 rpm, which is equivalent to a tip speed ratio (TSR) of about 2. More details about rotor models can be found in Öztürk et al. [17].

(a) (b) (c)

Figure 1. (a) Open-return suction type boundary layer wind tunnel at METU Center for Wind Energy Research (RÜZGEM), (b) Model wind turbine, and (c) porous disc.

2.2. Measurement Details

Wake measurements are performed under two inflow conditions, which are uniform inflow with low turbulence intensity and passive turbulence grid inflow, at a fixed Reynolds number of 100,000 based on turbine/disc diameter and freestream turbulence. Turbulence intensity levels within the test section at the rotor/disc hub position are measured as 0.5% and 4.5% for uniform inflow with low turbulence and passive turbulence grid inflow, respectively. The passive turbulence grid is designed by the methodology proposed by Roach [18]. Using hotwire data obtained at the model position for 30 seconds at a sampling rate of 10 kHz, the integral length scale is computed to be roughly 0.071 m. Further details can be seen in Öztürk et al. [17]. Both rotor models are placed 6 m downstream of the test section inlet and at the center of the test section. Both models are inserted from the side wall to minimize the tower effect on the wake. The wake measurements are conducted using two-dimensional two-component

particle image velocimetry (2D2C PIV) along the middle plane in the vertical direction (x-z plane) downstream of the wind turbine/porous disc. Figure 2-left shows the PIV configuration utilized for measurements. The PIV system consists of a Phantom v641 high-speed camera with a Nikon-Nikkor 60 mm lens, a New Solo PIV Nd:YAG laser, a Dantec Dynamics timer box, and Dynamic Studio data acquisition and analysis software. The laser, camera, and optics are mounted on a three-axis traverse mechanism to allow for easier measurement as we traverse them to cover the wake region. Seeding is provided with fog of droplets with a mean diameter of 1 μm. Double-frame particle images are pre-processed using a low-pass filter technique in order to enhance the image quality and remove any background noise. Then, a three-step adaptive-correlation analysis is used with the final interrogation window size of 32x32 pixels^2 and 50% overlap, a vector spacing of 1.58 mm is obtained in the resulting vector maps. Time between the two laser pulses is used as 80 μs.

Figure 2-right presents the field of views (FOVs) in the x-z plane, which are combined to obtain flow field downstream both the model wind turbine and the porous disc. The wake measurements are performed up to $0.5 \leq x/D \leq 7.0$ downstream of both models. The solid blue rectangle represents the wind turbine/porous disc with an exaggerated thickness. The grey shaded areas between the windows show the overlap regions between two adjacent FOVs, which is 0.12D (10%), corresponding to around ten vectors. The size of each field of view is 186 x 296 mm^2 (1.55D x 2.47D) along the streamwise and the vertical directions, respectively.

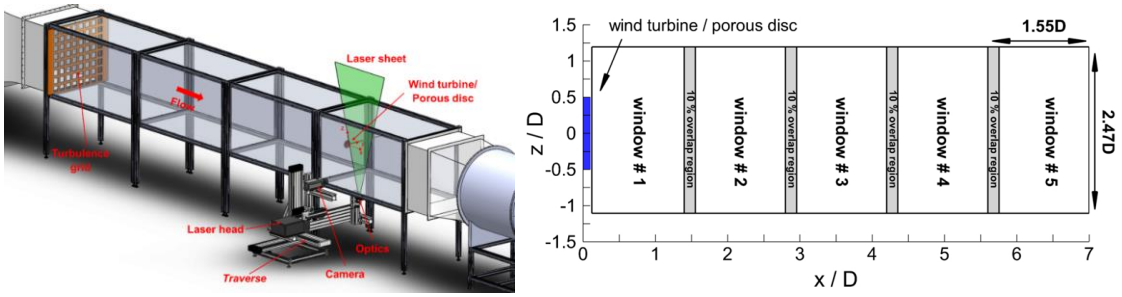

Figure 2. PIV measurement setup for wind turbine/porous disc wake measurements (left), and PIV measurement domain showing the windows with the overlap region and the field of view dimensions. The blue rectangular region represents the wind turbine/porous disc located between $-0.5 \leq z/D \leq 0.5$ (right).

2.3. Theory of Proper Orthogonal Decomposition

Snapshot Proper Orthogonal Decomposition (SPOD) is a statistical tool that breaks down space-time flow fields into discrete spatial modes and temporal coefficients, which is done by computing the major eigenvalue and eigenvector of a matrix composed of flow snapshots. Instantaneous velocity can be written as shown below, where u' (x,t) is the fluctuating velocity field [12]. Here, *x* is a vector composed of 2D spatial coordinates only since SPOD analysis is performed on 2D velocity fields obtained from planar (2D2C) PIV data for two velocity components (axial and radial), and *t* is the time at sample *m*.

$$U(x,t) = \bar{U}(x,t) + u'(x,t) \qquad (2.1)$$

Fluctuating vector field ($u'(x,t)$) can be decomposed into a series of deterministic spatial functions.

$$u'(x,t) = \sum_{m=1}^{M} a_m(t)\Phi^{(m)}(x) \qquad (2.2)$$

where $a_m(t)$ is the time-dependent POD coefficient for mode m, $\phi^{(m)}(x)$ is the spatial POD mode for mode m, and M is the number of snapshots [16]. A matrix composed of fluctuating velocity components measured at N spatial positions and M time instants can be formed as:

$$V = \frac{1}{M}\begin{bmatrix} u_1'^1 & u_1'^2 & \cdots & u_1'^M \\ \vdots & & \ddots & \vdots \\ u_N'^1 & u_N'^2 & \cdots & u_N'^M \end{bmatrix}$$

Then auto-covariance matrix (C) can be expressed as

$$C = V^T V \tag{2.3}$$

After the beforementioned steps, the eigenvalue problem can be introduced as follows.

$$CA = \lambda A \tag{2.4}$$

where A is the diagonal eigenvector matrix and λ is the diagonal eigenvalue matrix representing energy content where the calculated eigenvalues are ordered in magnitude as:

$$\lambda_1 > \lambda_2 > \cdots \lambda_m \tag{2.5}$$

The obtained modes through POD analysis not only depict the energy distribution but also give information about the spatial development of underlying dominant scales of motion.

3. Results

The snapshot POD technique is employed on the streamwise wake velocity of the model wind turbine and porous disc under two different freestream turbulent intensity conditions (i.e., 0.5% and 4.5%) in the near-wake ($0.5 \leq x/D \leq 1.5$, window # 1) and far-wake region ($4.6 \leq x/D \leq 5.8$, window # 4) as shown previously in Figure 2-right. For the sake of simplicity, here we refer to WT-ng and WT-g ('ng' for 'no grid' and 'g' for 'grid') stand for wind turbine cases operating at low and high freestream turbulence intensity levels, respectively. Likewise, PD-ng and PD-g refer to porous disc cases at low and high freestream turbulence intensity levels. POD analysis is conducted with M=1000 snapshots, which correspond to the acquired instantaneous flow field with 2D2C PIV for each case; therefore, a total of 1000 POD modes are obtained. Eigenvalues associated with the turbulent kinetic energy contribution representing these POD modes are sorted in reduced order.

Figure 3 presents the percentage turbulent kinetic energy distribution of the POD modes, which is the percentage ratio of the eigenvalue of a POD mode to the cumulative summation of eigenvalues. It can be seen that turbulent kinetic energy contribution decreases with increasing mode number, and the first few modes contain the majority of the total energy. In the near-wake region, the PD-g case has the highest first-mode energy contribution of both streamwise and radial components of POD (Figure 3a and 3c). For instance, the PD-g case has the highest first mode energy contribution for the streamwise component of POD with 18% while the percentage turbulent kinetic energy values are 11%, 10%, and 4% for the WT-g, PD-ng, and WT-ng cases, respectively. Results further show large differences in energy contribution between low and higher-order modes, except the WT-ng case, which has almost evenly distributed energy contribution, especially for streamwise modes. Thus, a few low-order modes contribute a big part of total kinetic energy. To illustrate, the turbulent kinetic energy contribution of the first five radial modes of PD-g and WT-g cases correspond to 51% and 48%, respectively. In addition, it is shown that the percentage of kinetic energy contribution of the cases under higher freestream turbulence intensity conditions is larger compared to cases operating at low freestream turbulence intensity. Furthermore, it seems that percentage turbulent kinetic energy distribution of both streamwise and radial modes of the PD-ng and PD-g cases seem almost identical (Figure 3b and 3d), and the energy content of the first three radial modes of the WT-g case is higher compared to other cases. Similar in the near-wake region, energy contents of both POD components for all cases significantly drop as the order of modes increases. The convergence of the POD modes associated with the axial and radial velocities is tested by comparing the percentage turbulent kinetic energy contribution of the first five modes of selected cases with an increasing number of snapshots obtained from 2D2C PIV measurements. In order to perform the analysis, 50, 250, 500, 750, and 1000 snapshots are used to evaluate the modes. Figure 4 presents the results, which depict a good level of convergence when 1000 snapshots are employed.

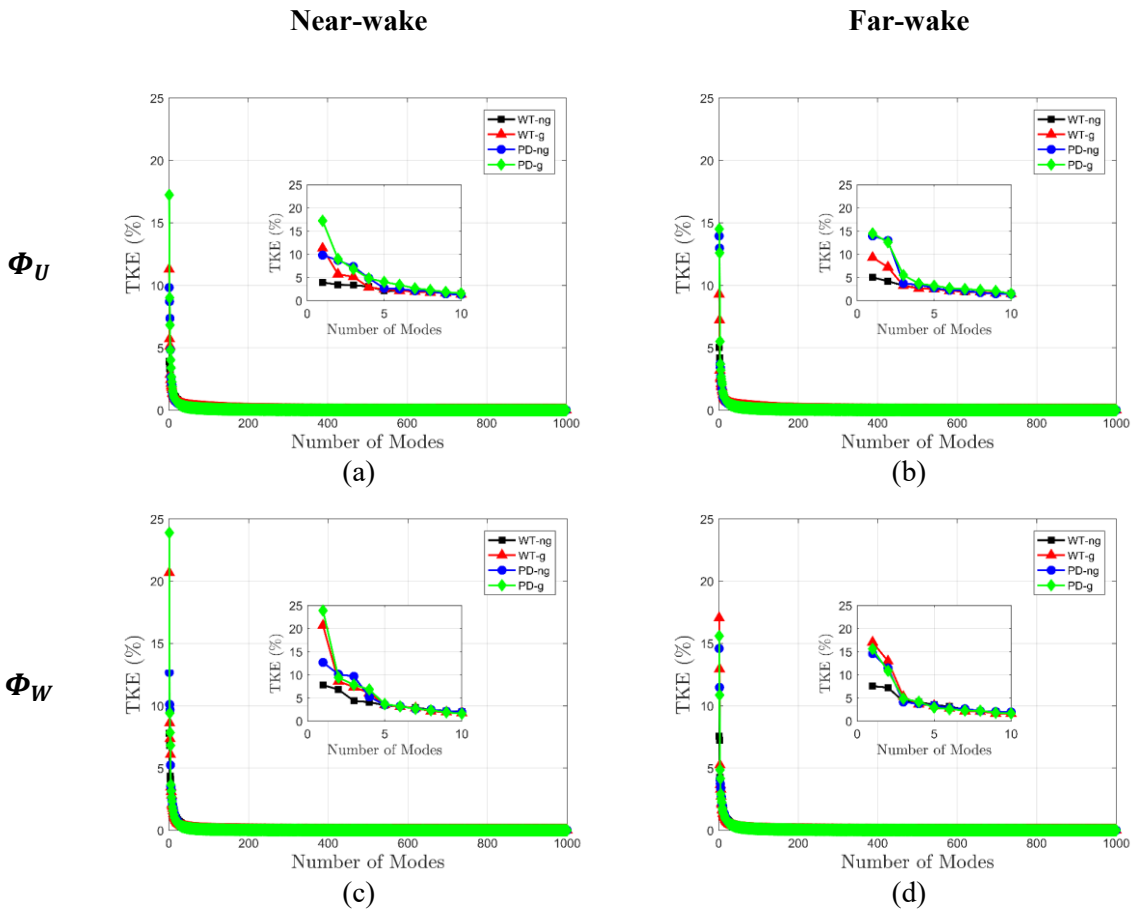

Figure 3. Distribution of percentage of turbulent kinetic energy (TKE) attributed to eigenvalues (a,c) in the near-wake and (b,d) in the far-wake of the model wind turbine and the porous disc cases. (a,b) Streamwise components of POD modes (Φ_U) and (c,d) radial components of POD modes (Φ_W) are presented in the first and second rows, respectively.

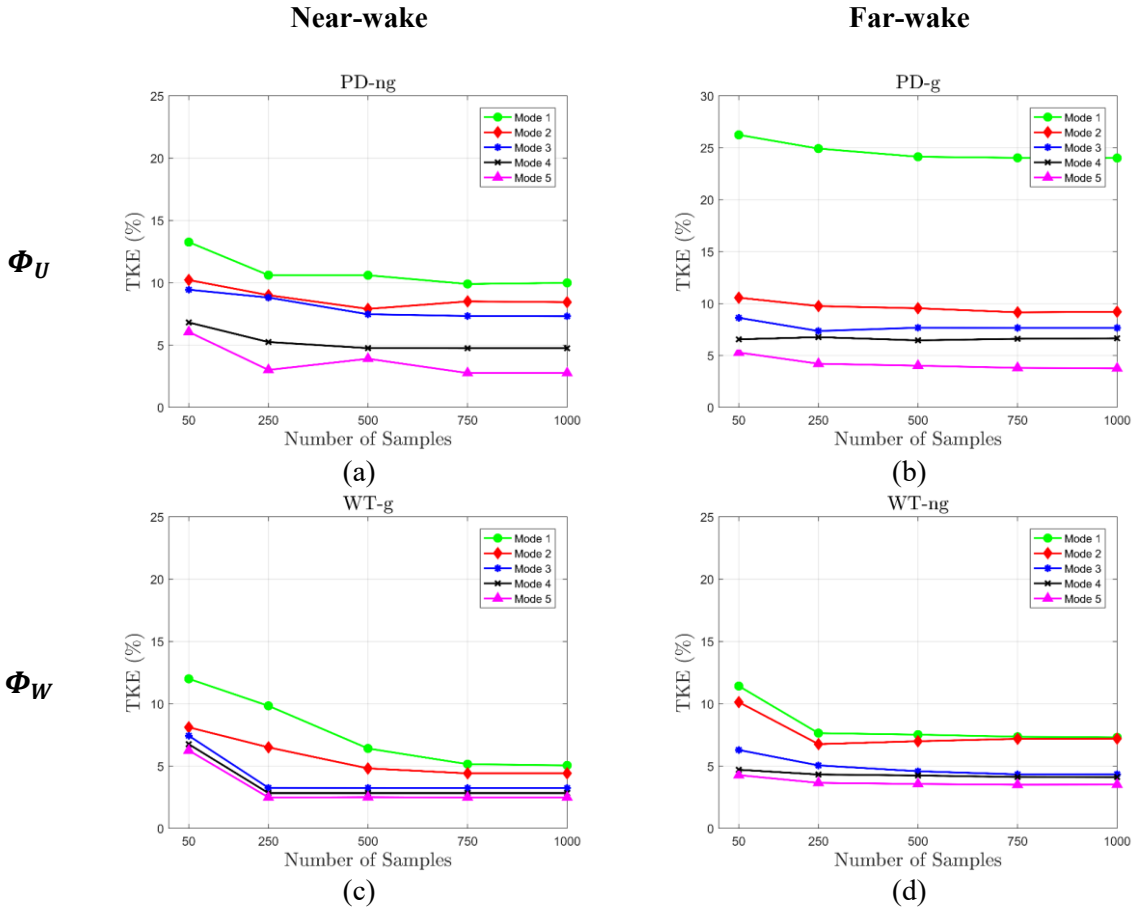

Figure 4. Percentage turbulent kinetic energy (TKE) convergence of selected cases in the near-wake region (a,c) and in the far-wake region (b,d) using different numbers of samples obtained from 2D2C PIV.

Figure 5 shows the first five streamwise POD modes of all four cases in the near-wake region. Streamwise elongated coherent structures occur between two tip positions of wind turbine/porous disc in the z-direction ($-0.5 \leq z/D \leq 0.5$). Results show that the coherent structures of the first modes, which have the highest percentage cumulative distribution of turbulent kinetic energy, are not similar for the WT-ng and PD-ng cases. However, one can observe similar structures of first modes for WT-g and PD-g cases, which are comparable with those in Camp and Cal [9]. Furthermore, one can observe similar second modes for all cases which are related to the Karman vortices shed by the tower [15]. Similarities between coherent structures of higher modes for WT-ng and PD-ng cases lessen where the ambient turbulence intensity level is lower. On the other hand, coherent structures become comparable, and more POD modes can be matched as freestream turbulence intensity increases when comparing the first four modes for WT-g and PD-g cases. It can be seen that all first four modes of WT-g and PD-g cases can be directly matched. It is worth noting that this is an interesting outcome since a wind turbine and a porous disc have completely different wake development characteristics in the near-wake region. Tip vortices form and reduce the kinetic energy entrainment in the near-wake of a wind turbine, while they are absent due to the lack of rotation within the wake of a porous disc, and turbulent mixing is more pronounced [4]. It seems that higher freestream turbulent intensity influences the coherent structures within the wake of both models in a way that they become more comparable.

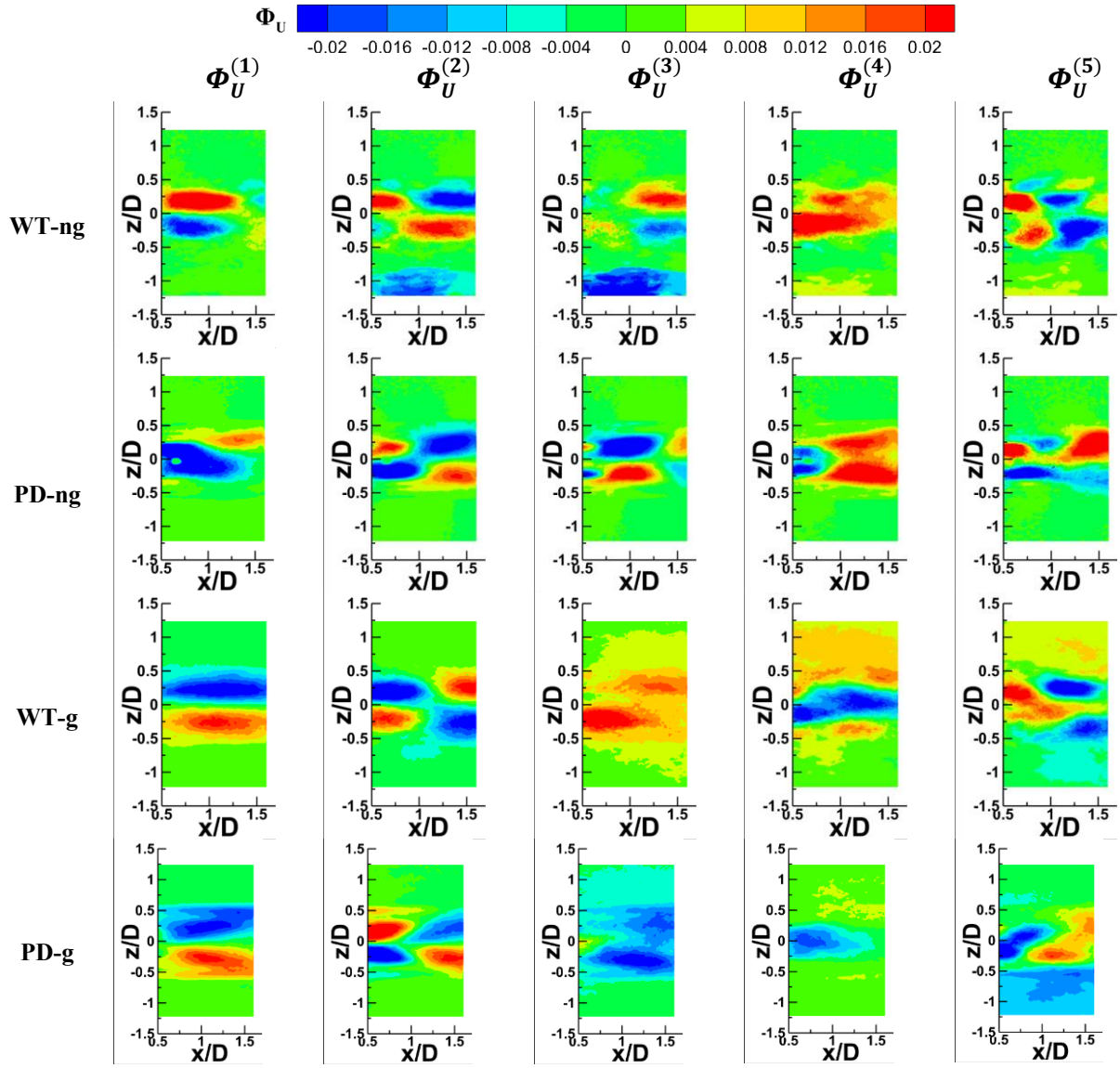

Figure 5. The first five streamwise POD modes (Φ_U) in the near-wake of the model wind turbine and the porous disc at different freestream turbulence intensity levels.

Figure 6 presents the first five streamwise components of POD modes of all four cases in the far-wake region. One can observe that coherent structure size increases and larger streamwise elongated features are evident at higher inflow turbulence conditions, which is an outcome in accordance with the findings of Cherubini [19]. When comparing wind turbine cases (WT-ng and WT-g), it is observed that the first two POD modes match, while there are no comparable modes for porous disc cases under both freestream turbulence intensity levels (PD-ng and PD-g). On the other hand, as previously observed in the near-wake region, similar POD modes are evident at higher freestream turbulence intensity. All five modes for the WT-g and PD-g cases match in structure except for the order shift in the second and third modes, which operate under high turbulence intensity conditions. In this manner, it is more likely to expect coherent structures associated with similar energy contributions to become more similar when the freestream turbulence intensity level is higher in the far-wake region where the wakes of both model decay and freestream turbulence become the dominant factor.

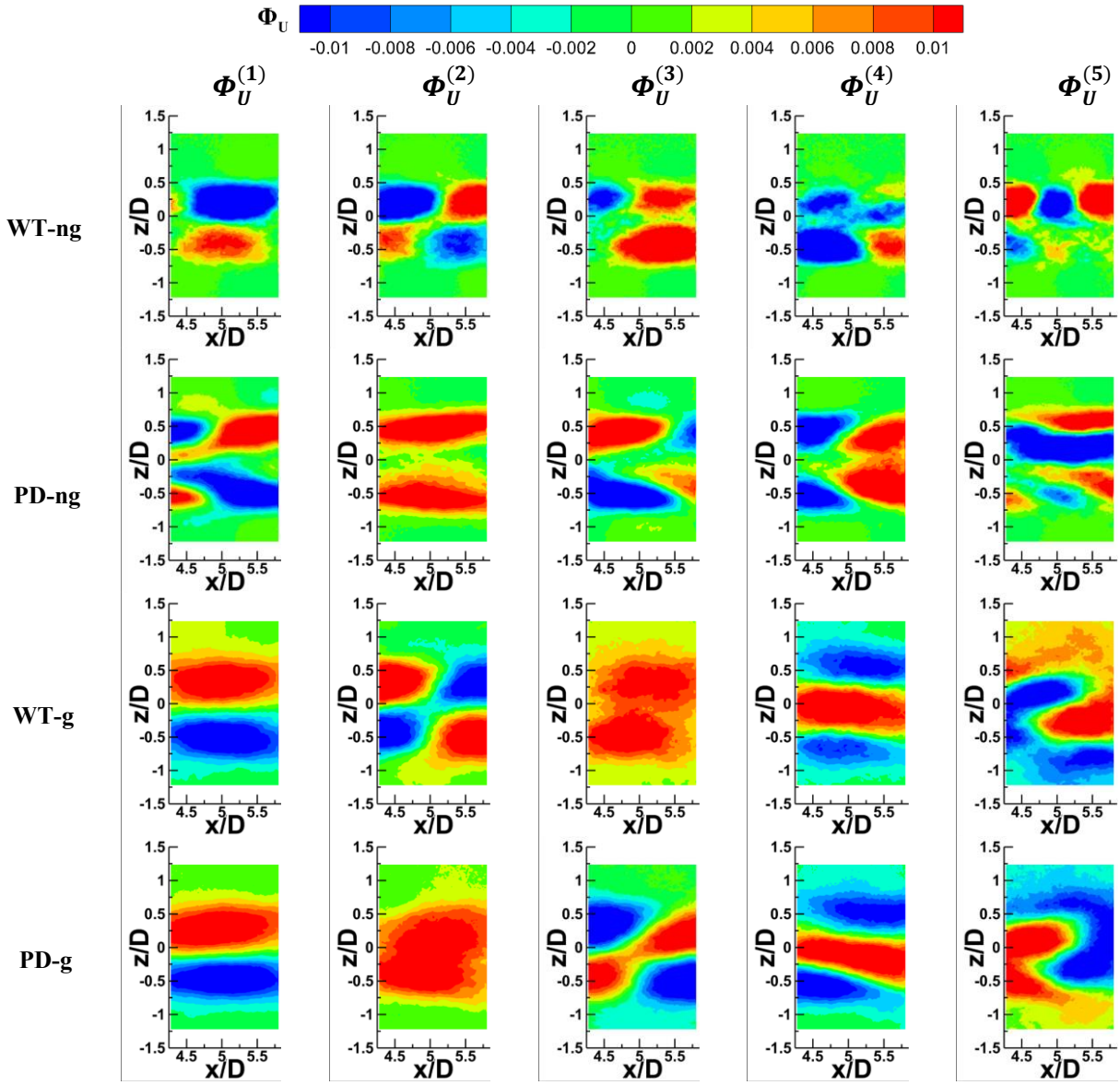

Figure 6. The first five streamwise POD modes (Φ_U) in the far-wake of the model wind turbine and the porous disc at different freestream turbulence intensity levels.

The first five radial components of POD modes of all cases in the near-wake region are shown in figure 7. Results reveal that the first two modes, comparable with Camp and Cal [9], have similar coherent structures for all cases despite an order shift for the WT-g case. In addition, comparable structures of higher-order modes are evident for wind turbine cases except for the third mode for the WT-g case. Furthermore, features of POD modes with the same order (third, fourth, and fifth) are not matching for porous disc cases. On the other hand, results demonstrate matching modes, which are the third modes of WT-g and PD-g cases, when freestream turbulence intensity is higher. Nevertheless, sixfold features observed in higher-order vertical modes seem specific for wind turbine cases, which can be related to vortex shedding.

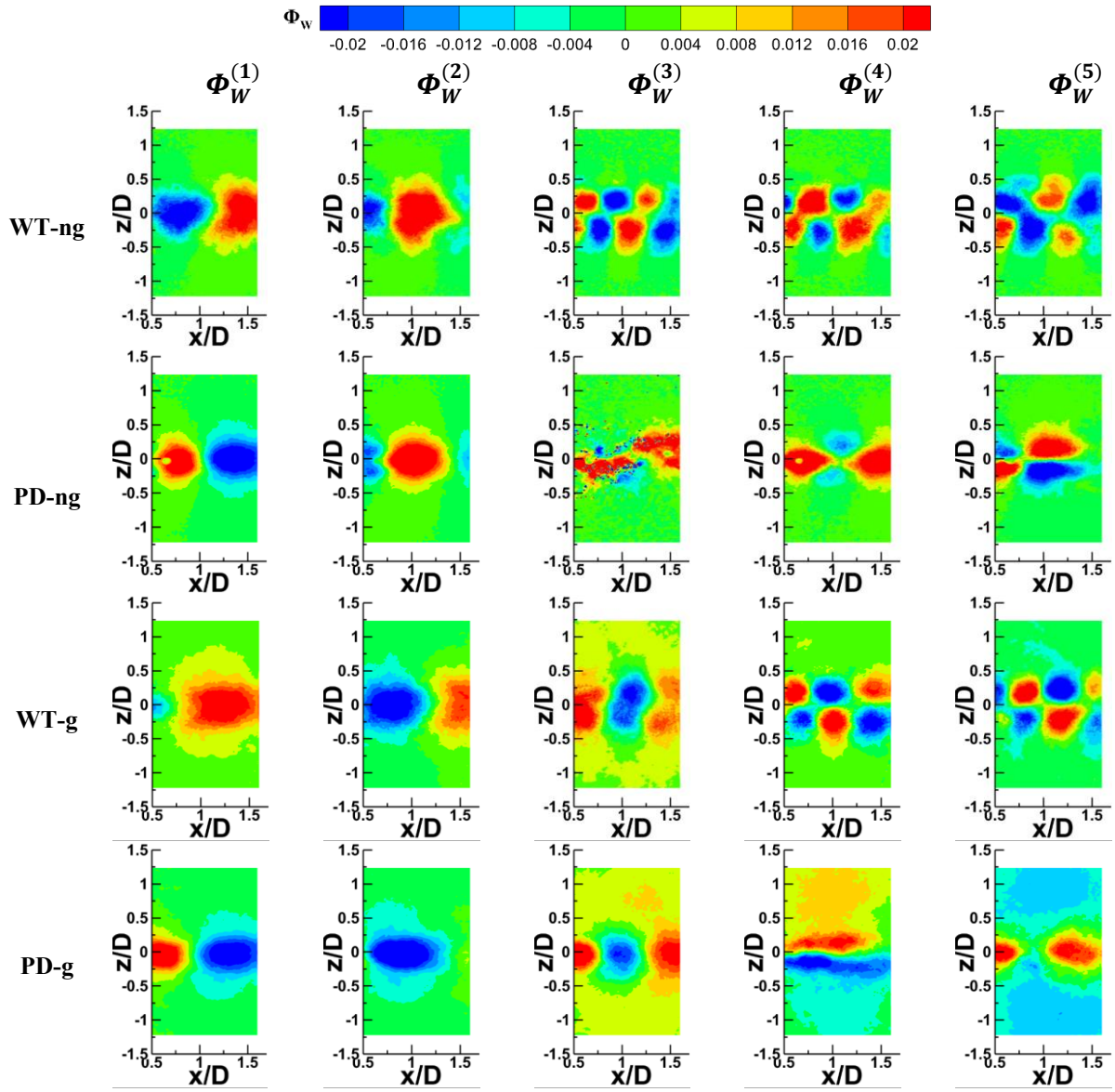

Figure 7. The first five radial components of POD modes (Φ_V) in the near-wake of the model wind turbine and the porous disc at different freestream turbulence intensity levels.

Figure 8 presents POD modes based on vertical velocity components in the far-wake region. Results show that coherent structures generally observed in the first three POD modes occupy the region between the tip positions for all cases, which was previously observed by Andersen et al. [13]. Common to the discussion of the effects of inflow turbulence intensity levels on the coherent structures of the wake flow over the current study, it is apparent that more POD modes for the model wind turbine and porous disc are matching under higher ambient turbulence intensity conditions. One can observe that all five modes for the WT-g and PD-g cases (except the third and fourth mode for the PD-g) are comparable.

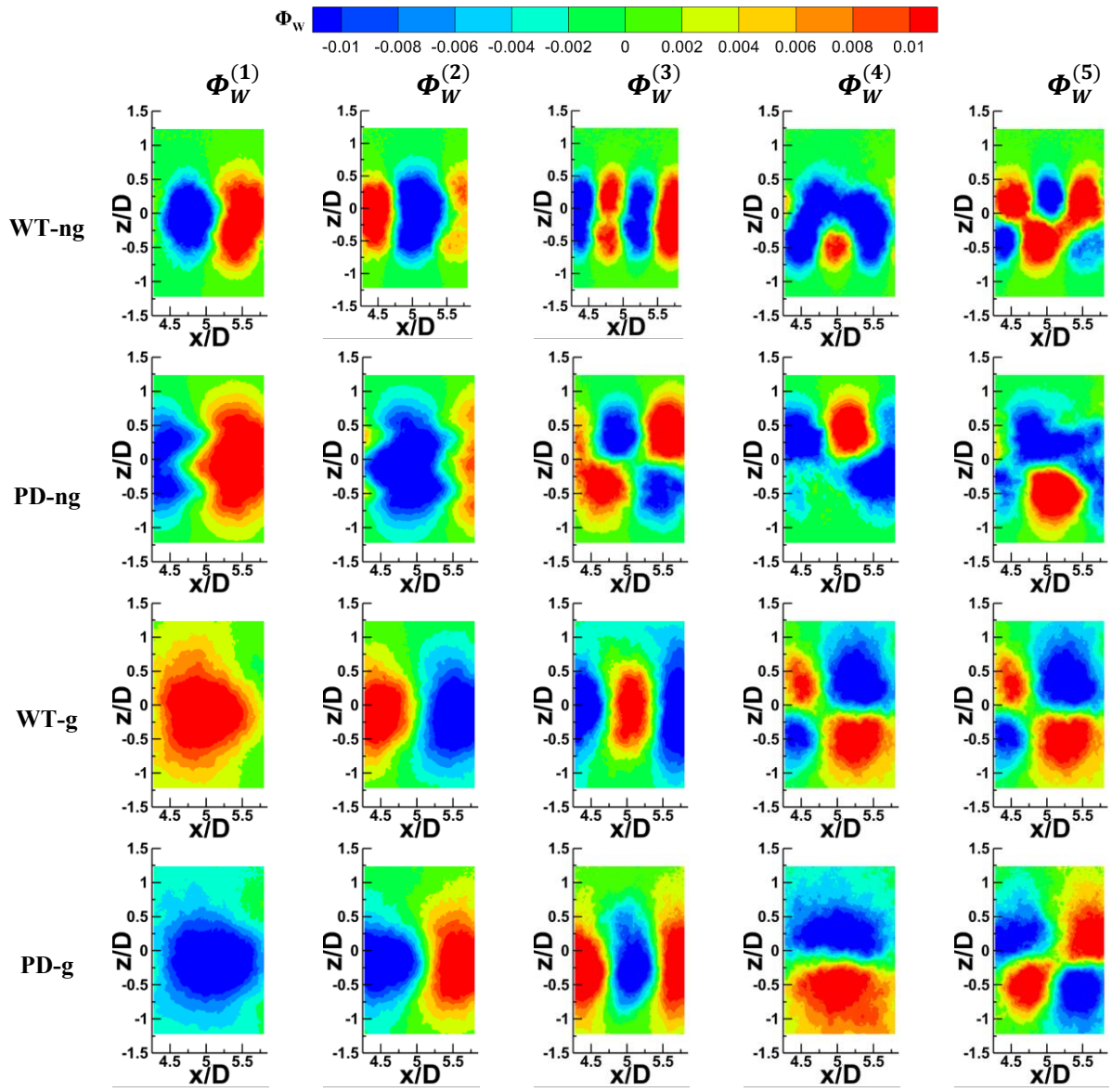

Figure 8. The first five radial components of POD modes (Φ_V) in the far-wake of the model wind turbine and the porous disc at different freestream turbulence intensity levels.

4. Conclusions

A comparative experimental study on the freestream turbulence effects on the wake development characteristics of a model wind turbine and a porous disc with a comparable thrust coefficient is presented. Proper Orthogonal Decomposition analysis is employed to analyze differences between the wake characteristics of both models within the near and far wake regions by comparing coherent structures. Results show that number of matching POD modes, both axial and vertical components, is limited when ambient turbulence is lower. On the other hand, when both the model wind turbine and porous disc operate under turbulent inflow, more matching modes are observed since the large-scale coherent structures carried by turbulent inflow reduce the effects of tip and root vortices on the wake development of wind turbine [20]. In other words, mixing mechanism differences, especially within the near-wake region, between the two experimental models diminish, and the rate of wake recovery increases for both model wind turbine and porous disc as a result of turbulent mixing. This outcome

indicates the influence of freestream turbulence on the wake development of a non-rotating rotor model and enhances the ability to replicate far-wake characteristics of a model wind turbine. It is shown that when employing porous discs to replicate wind turbines in wind tunnel studies, care should be taken in selecting the freestream turbulence intensity level.

References

[1] Vermeer L J, Sørensen J N and Crespo A 2003 Wind turbine wake aerodynamics Prog. Aerosp. Sci. 39 467–510
[2] Barthelmie R J, Courtney M S, Højstrup J and Larsen S E 1996 Meteorological aspects of offshore wind energy: Observations from the Vindeby wind farm J. Wind Eng. Ind. Aerodyn. 62 191–211
[3] Wu Y T and Porté-Agel F 2012 Atmospheric turbulence effects on wind-turbine wakes: An LES study Energies 5 5340–62
[4] Medici D and Alfredsson P H 2006 Measurements on a wind turbine wake: 3D effects and bluff body vortex shedding Wind Energy 9 219–36
[5] Andersen S. J., Lignarolo L. E. M., Ragni D., Simao Ferreira C. J., Sorensen J. N., Mikkelsen R. F., van Bussel G. J. W. 2014 Comparison between PIV measurements and computations of the near-wake of an actuator disc Journal of Physics: Conference Series 524 (2014) 012173.
[6] Aubrun S, Loyer S, Hancock P E and Hayden P 2013 Wind turbine wake properties: Comparison between a non-rotating simplified wind turbine model and a rotating model J. Wind Eng. Ind. Aerodyn. 120 1–8
[7] Camp E H and Cal R B 2016 Mean kinetic energy transport and event classification in a model wind turbine array versus an array of porous disks: Energy budget and octant analysis Phys. Rev. Fluids 1
[8] Lignarolo L E M, Ragni D, Ferreira C J and Van Bussel G J W 2016 Experimental comparison of a wind-turbine and of an actuator-disc near wake J. Renew. Sustain. Energy 8
[9] Camp E H and Cal R B 2019 Low-dimensional representations and anisotropy of model rotor versus porous disk wind turbine arrays Phys. Rev. Fluids 4 24610
[10] Lumley J L 1967 The structure of inhomogeneous turbulent flows," in "Atmospheric turbulence and radio wave propagation
[11] Lumley J L 1981 Coherent Structures in Turbulence Transition and Turbulence ed R E MEYER (Academic Press) pp 215–42
[12] Sirovich L 1987 Turbulence And The Dynamics Of Coherent Structures Part I: Coherent Structures Q. Appl. Math. 45 561–71
[13] Andersen, S. J., Sørensen, J. N., and Mikkelsen, R., 2013. Simulation of the inherent turbulence and wake interaction inside an infinitely long row of wind turbines. Journal of Turbulence, 14. 1-24, 2013. https://doi.org/10.1080/14685248.2013.796085.
[14] VerHulst C., and Meneveau, C. 2014. Large eddy simulation study of the kinetic energy entrainment by energetic turbulent flow structures in large wind farms. Physics of Fluids, 26. 025113. https://doi.org/10.1063/1.4865755.
[15] De Cillis G, Cherubini S, Semeraro O, Leonardi S and De Palma P 2021 POD-based analysis of a wind turbine wake under the influence of tower and nacelle Wind Energy 24 609–33
[16] Bastine, D., Witha, B., Wächter, M., and Peinke, J. 2015. Towards a simplified dynamic wake model using POD analysis. Energies, 8. 895-920. https://doi.org/10.3390/en8020895.
[17] Öztürk B, Hassanein A, Tuğrul Akpolat M, Abdulrahim A, Perçin M and Uzol O 2022 Effects of freestream turbulence on the wake growth rate of a model wind turbine and a porous disc J. Phys. Conf. Ser. 2265 022042
[18] Roach P E 1987 The generation of nearly isotropic turbulence by means of grids Int. J. Heat Fluid Flow 8 82–92
[19] Cherubini S, Cillis G De, Semeraro O, Leonardi S and Palma P De 2022 How incoming turbulence affects wake recovery of an NREL-5MW wind turbine J. Phys. Conf. Ser. 2385

[20] De Cillis G, Cherubini S, Semeraro O, Leonardi S and De Palma P 2022 The influence of incoming turbulence on the dynamic modes of an NREL-5MW wind turbine wake Renew. Energy 183 601–16